JOURNAL OF PROPULSION AND POWER
Vol. 22, No. 2, March–April 2006

Trailing-Edge Cooling for Gas Turbines

F. J. Cunha
Pratt and Whitney Aircraft, United Technologies Corporation, East Hartford, Connecticut 06108
and
M. K. Chyu
University of Pittsburgh, Pittsburgh, Pennsylvania 15261

The trailing-edge section of modern high-pressure turbine airfoils is an area that requires a high degree of attention from turbine performance and durability standpoints. Aerodynamic loss near the trailing edge includes expansion waves, normal shocks, and wake shedding. Thermal issues associated with trailing edge are also very complex and challenging. To maintain effective cooling ensuring metal temperature below design limit is particularly difficult, as it needs to be implemented in a relatively small area of the airfoil. To date, little effort has been devoted to advancing the fundamental understanding of the thermal characteristics in airfoil trailing-edge regions. Described in this paper are the procedures leading to closed-form, analytical solutions for temperature profile for four most representative trailing-edge configurations. The configurations studied are 1) solid wedge shape without discharge, 2) wedge with slot discharge, 3) wedge with discrete-hole discharge, and 4) wedge with pressure-side cutback slot discharge. Comparison among these four cases is made primarily in the context of airfoil metal temperature and resulting cooling effectiveness. Further discussed in the paper are the overall and detail design parameters for preferred trailing-edge cooling configurations as they affect turbine airfoil performance and durability. Also described in this treatment is a current experimental investigation of heat transfer over a trailing-edge configuration. The trailing edge is preceded with an internal cooling channel of pedestal array. The pedestal array consists of both circular pin fins and oblong shaped features or exit teardrops. Downstream to the pedestal array, the trailing edge exits in a pressure side cutback partitioned by the oblong-shaped teardrops. The local heat-transfer coefficient over the entire wetted surface in the internal cooling chamber has been determined using a "hybrid" measurement technique based on transient liquid crystal imaging. The hybrid technique employs the transient conduction model in a semi-infinite solid for resolving the heat-transfer coefficient on the end-wall surface uncovered by the pedestals. The heat-transfer coefficient over a pedestal can be resolved by the lumped capacitance method with an assumption of low Biot number. The overall heat transfer for both the pedestals and end-walls combined shows a significant enhancement compared to the case with thermally developed smooth channel. Near the most downstream section of the suction side, the land, caused by pressure side cutback, is exposed to the stream mixed with hot gas and discharged coolant. Both the adiabatic effectiveness and heat-transfer coefficient on the land section are characterized by using this hybrid liquid-crystal technique.

Dr. Cunha is a Principal Engineer at Pratt & Whitney responsible for advanced turbine designs of commercial and military engine programs. Dr. Cunha is also responsible for establishing technical direction for a consortium of Universities as well as in-house research programs in the area of state-of-the-art cooling technologies suitable for use with extremely aggressive gas turbine rotor inlet temperatures. Dr. Cunha's professional career spans a period of 27 years with turbine original equipment manufacturers including General Electric and Siemens. Dr. Cunha has authored numerous technical papers and gas turbine design standards. Dr. Cunha holds 21 U.S. patents in turbomachinery and is presently a member of the IGTI-ASME heat transfer committee.

Dr. Minking K. Chyu is presently the Leighton Orr Chair Professor and Chairman of mechanical engineering department at the University of Pittsburgh. He received his Ph.D. degree from the University of Minnesota in 1986. He was a faculty member at Carnegie-Mellon University for 14 years before joining the University of Pittsburgh in 2000. His primary research area lies in thermal issues ralating to power and propulsion systems. He has conducted research projects sponsored by a number of government agencies and industry. Professor Chyu is a Fellow of the American Society of Mechanical Engineers (ASME), Associate Fellow of American Institute of Aerospace and Aeronautics and a member of the Scientific Council of the International Centre of Heat and Mass Transfer (ICHMT). He was named the Engineer of the Year by the ASME Pittsburgh Chapter in 2002. He serves as an Associate Editor for the *Journal of Heat Transfer*, ASME and a Foreign Editor for the *Journal of Chinese Society of Mechanical Engineers*.

Received 4 November 2005; accepted for publication 6 November 2005.

Nomenclature

A = area
C_p = fluid specific heat at constant pressure
c = specific heat
D = diameter
d = pin diameter
E = cooling parameter
f = friction factor
g_c = gravitational constant
H = trailing-edge height at the base
h = heat-transfer coefficient
I_0 = Bessel function of second kind, order zero
J = mechanical to thermal energy conversion factor
k = thermal conductivity
L = length
M = slope parameter, blowing ratio
m = flow rate
N = number of cooling openings
Nu = Nusselt number
n = number of pins
P = perimeter
Pr = Prandtl number
Re = Reynolds number
r = radius
S = sink parameter
s = slot height
T = temperature
t = time or thickness
Q = total heat transfer
q = heat flux
U = velocity, step change
u = trailing-edge slope parameter
V = velocity
W = width
x = axial distance
y = $L - x$
z = distance normal to the surface
α = thermal diffusivity
Δ = finite change
δ = small change
η = film effectiveness
θ = dimensionless temperature
μ = viscosity
ρ = density
τ = time
ϕ = cooling effectiveness
ω = speed

Subscripts

aw = adiabatic wall
B = bottom
b = base
c = coolant, constant
d = pin diameter
f = coolant flow
g = gas
H = holes, height
i = initial
m = main flow
o = baseline
p = along transverse pitch
r = reference
S = surface
T = top
w = wall

Introduction

IN modern high-pressure turbine airfoils, the aft section of the airfoil denoted as the trailing-edge section is an area that requires a high degree of attention from turbine designers and researchers. This is particularly true because of the fundamental role that airfoil trailing edges have on the overall design of all turbines in operation today for aircraft engines and electrical generating powerplants.

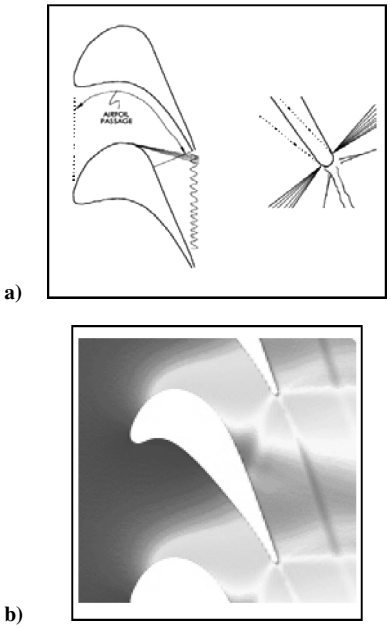

Fig. 1 Typical shock structures in high-pressure turbine airfoils: a) from Kuhne[1] and b) from Eisemann.[2]

Airfoil trailing edges provide a degree of blockage in the gas flowpath contributing to the overall degradation of turbine performance and efficiency. Along the turbine airfoil external walls, there are pressure profiles on the pressure (concave) and suction (convex) sides, which lead to pressure differences between the pressure and suction sides at the airfoil trailing edge. These pressure profiles result in expansion waves in blade passage, trailing-edge normal shocks, and wake shedding as illustrated in Fig. 1 (Refs. 1 and 2). All of these effects contribute to increasing turbine losses. Thus, the illusive theoretical goal of the aerodynamic Kutta condition,[3] requiring the gas flow to leave the airfoils smoothly at the trailing edge is impossible to achieve with today's technology and cooling requirements. The thickness of airfoil trailing edges is directly related to the turbine aerodynamic performance as it affects the gas-path aerodynamic losses. Airfoil cooling in this region is also extremely difficult to achieve, as it needs to be implemented effectively in a relatively small area of the airfoil. Without cooling, however, the trailing-edge metal temperatures would reach metal temperatures higher than the melting temperatures of most superalloys.

Innovative ideas are required to obtain the most practical and effective means to cool these airfoil regions. Low or inadequate trailing-edge cooling can lead to high thermal strains, as airfoil trailing edges respond thermally faster than other parts of the airfoil. This is caused by the heat capacity of relatively small trailing-edge mass when compared to the rest of the airfoil. Resulting thermal mismatch within the airfoil walls can lead to excessive thermal-mechanical cyclic loading, which can be exacerbated with long dwell times at high temperatures during climbing, cruising, and continuous power generation for aircraft and land-based turbines.

Current cooling technology for gas-turbine trailing edges relies primarily on the coolant air induced from the airfoil main-body upstream. As the coolant reaches the trailing edge, it might have limited heat capability removal. As a result, passive heat-transfer enhancement features need to be implemented in this region. One type of cooling channel near the trailing edge is an open chamber with cylindrical pedestals connecting opposed suction- and pressure-side walls. These pedestals are generally arranged in a staggered array to promote convective heat transfer in the chamber. However, cylindrical pedestal features are often subject to concentrated thermally induced stress. Because the pressure-side external thermal load is

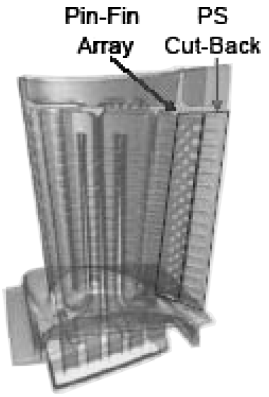

Fig. 2 Cutaway view of turbine blade, from Martini et al.[4]

higher than that of the suction side, there is more thermal expansion on the pressure side. This is particularly the case near the root region immediately adjacent to the platform, where the temperature differential between the two airfoil side surfaces is more substantial. To alleviate such stress, while still maintaining sufficient level of heat-transfer enhancement, some of the cylindrical pedestals are replaced by shaped, filleted, and often larger-sized pedestals.

Figure 2 shows a cutaway view of a blade illustrating the trailing-edge configuration. As depicted in this figure, the part to the right of the exit of the internal cooling chamber is pressure-side cutback area, which is equally spaced by the oblong shaped features, also known as trailing-edge exit teardrops. These oblong-shaped teardrops also provide structural integrity for the blade. From a phenomenological point of view, creep growth can occur close to the apex of the trailing edge. Nearby thermal strains give rise to stress intensities and subsequent trailing-edge thermal-mechanical cracking nucleation. As the centrifugal force remains constant, the colder portions of the airfoil begin sharing the load as the hottest portions of the blade start the process of stress relaxation. This interaction is commonly referred to as the airfoil load shakedown.[5] Load sharing could eventually lead to a state of potential overstress in the cold regions of the airfoil with substantial plastic deformation. The interaction of events can eventually culminate in catastrophic structural failure. Attention is thus required in the design process to avoid exceeding the endurance limits of the material. This is a major concern for turbine designers and researchers as airfoils are designed fundamentally using deterministic means for crack initiation before crack propagation.[6]

Advances in material science have continued along with advances in blade-cooling technology for airfoil trailing-edge designs. Materials of construction for these airfoils have, therefore, become an important part of material science development and testing. As the rotor inlet temperatures have increased in the last 20 years, there have been considerable advances in alloy composition and casting technology. Early equi-axed nickel and cobalt alloys have been displaced by single-crystal nickel superalloys for the most advanced military and commercial gas-turbine engines. Even in land-based power-generation turbines, directionally solidified and single-crystal alloy castings are now finding their way as first-stage turbine components. Similarly, to these developments, metallic and thermal barrier coatings have excelled and are regarded as prime-reliant features in all advanced turbine designs. Even with these advances, the oxidation, creep, and fatigue resistance of trailing edges are still being challenged by the adverse and compounding effects of vibrational stresses. These dynamic effects occur in extreme hot rotating environments with harmonically varying pressure fields.

To bring trailing-edge designs within the available design space, several fabrication methods are used today. These include 1) internal cooling schemes to bring the metal temperature within design limits; 2) internal aluminide coatings to prevent internal oxidation; 3) external metallic bond coatings to prevent external oxidation and aluminum content depletion; 4) thermal barrier coatings to reduce external thermal loading; 5) structural design features and devices integrated in the cooling schemes to reduce thermal, bending, panel, and vibratory stresses; and 6) optimization of trailing-edge thickness and airfoil wedge angles to minimize film-cooling degradation and aerodynamic losses. All of these aspects need to be assembled together to balance the design and satisfy the stringent design requirements in terms of heat transfer, structures, and performance.

Unlike the case for airfoil main-body cooling, the research concerning trailing-edge cooling is rather limited. This is particularly the case for geometry involving pressure-side cutback. Taslim et al.[7] investigated the film-cooling effectiveness downstream of trailing-edge slots disrupted by lands in the transverse direction. The influences of density ratio, lip thickness, slot width, and ejection angles were examined. In line with some earlier findings,[8–11] they suggested that lip-to-slot ratio is a key parameter for film cooling on cutback surfaces. The other important finding observed in their study is that the adiabatic effectiveness for a given blowing ratio is virtually insensitive to density ratio and slot width. But it was found sensitive to the injection angle, with an optimum angle about 8.5 deg. More recently, Uzol and coworkers[12,13] studied the discharge behavior of different trailing-edge slot at varying lengths of the cutback surface in a scaled-up subsonic cascade. Their results from particle image velocimetry and total pressure measurements in the wake region suggested that trailing edges with pressure-side cutback induced smaller aerodynamic loss than those without pressure-side cutback. Holloway et al.[4,14] numerically investigated flow and heat transfer in a trailing-edge slot with disrupted lands under realistic engine conditions. Their simulation reveals periodic vortex shedding when the lip-to-slot ratio $t/s = 0.9$. This vortex shedding might be involved in the relatively fast decay of film-cooling effectiveness for slots with larger t/s. Chyu et al.[15] reported a study concerning internal heat transfer in a triple-cavity structure trailing edge. They reported that the heat-transfer enhancement level in such a configuration is nearly 50% lower than that for the pedestals or pin fins when $Re > 20{,}000$. Martini and Schulz[16] examined a trailing-edge slot equipped with an internal rib array featuring a small lateral pitch of 2. Their experimental and numerical efforts showed a phenomenon of regrouping of coolants jet that are of significant impact on trailing-edge pressure-side cutback film-cooling effectiveness. Kim et al.[17] studied the effect of mainstream acceleration on the film-cooling effectiveness and heat transfer in trailing edge with pressure-side cutback. Their results indicated that both local heat-transfer coefficients and film-cooling effectiveness exhibited a strong dependency on blowing ratio and mainstream acceleration. Lately, Martini et al.[18] measured the cooling effectiveness and heat transfer on the trailing-edge cutback of gas-turbine airfoils with different internal cooling designs. The designs included double in-line rib array, equilaterally staggered cylindrical pin arrays, and equilaterally staggered cylindrical pin arrays with lip overhang. Their results indicated that the extension of the core region where the film effectiveness η is close to unity is influenced strongly by the internal cooling design, whereas the decay of η downstream of the core region is similar for all trailing-edge cooling slots. The internal cooling design mainly affects the region $x/s < 5$, while the influence of the blowing ratio extends further downstream. Cunha et al.[19] presented closed-form, analytical solutions for temperature profile for four most representative trailing-edge configurations. These solutions will be detailed in this article for reference. They also discussed the overall and detail design parameters for the preferred trailing-edge cooling configurations.

One of the most unique features inherited in the present problem associated with Fig. 2 is that the cooling mechanism over the entire system is a combination of internal cooling and external cooling. Specifically, the internal cooling takes places in the cooling chamber that houses the pedestal array. On the other hand, the external cooling prevails in the cutback area. For research investigations, the heat transfer in the cutback area subjected to slot film protection is characterized as essentially a "three-temperature" convection problem, as the thermal transport in the region is determined by 1) the wall temperature, 2) mainstream temperature, and 3) slot-film discharge temperature. In addition to the heat-transfer coefficient, a new reference temperature, such as adiabatic temperature or dimensionless film effectiveness, needs to be determined also. A detailed method in resolving three-temperature problems can be found in Refs. 20–24.

In this study, attention will be focused on two fundamental building blocks for assessing cooling in gas-turbine trailing edges. The first building block presents an analytical development, whereas the second building block presents an experimental setup and procedures currently used for assessing the heat transfer and film effectiveness associated with gas-turbine trailing-edge regions. In the analytical development, four of the most representative configurations will be introduced to analyze their relative merits in terms of durability. As such, the interplay between geometrical features and airfoil metal temperatures will be described and explained using closed-form, analytical models. Trailing-edge cooling schemes will be presented in the context of metal temperature or resulting cooling effectiveness, as it affects all other design parameters, including creep, thermal-mechanical fatigue, oxidation, spallation, and performance. The four configurations studied are 1) solid wedge shape without discharge, 2) wedge with slot discharge, 3) wedge with discrete-hole discharge, and 4) wedge with pressure-side cutback slot discharge. In the experimental domain, a hybrid measurement technique is presented. The hybrid denomination arises from the contribution of two different test procedures: 1) the one-dimensional transient liquid-crystal technique for surface uncovered by pedestals and 2) one lumped heat capacity liquid-crystal technique for the heat transfer over pedestal surfaces.

Analytical Models

The underlying consideration for the models developed in this section is the one-dimensional nature of the heat transfer verified at the airfoil trailing-edge regions of operational blades and vanes. In this way, the heat-flux vectors are considerably normal to the trailing-edge surface with very little lateral heat flux. These considerations have been confirmed in hardware design. The setup of thermal boundary conditions for the model can be a very laborious process. On the external side, computational fluid dynamic can be used to set up external pressure and Mach-number distributions with a set of turbulence intensity levels as shown in Fig. 1. Boundary programs are used to establish the external heat-transfer coefficients based on expected wall roughness and airfoil curvature. The evaluation of these coefficients is not the purpose of this paper, and, as a result, representative values are provided as boundary conditions to the analytical models. Similarly, the same procedure is followed for the gas temperatures that are usually determined from previous film-cooling tests. Different coating systems can also be modeled as modified equivalent heat-transfer coefficients. Inside the airfoil, flow network tools can be used to determine internal pressure drops, internal fluid temperatures, and Mach-number distributions. Heat-transfer correlations are also based on previous testing to provide the means to evaluate internal heat-transfer coefficients. With known external and internal conditions, the following analytical models can be used to study different airfoil trailing-edge configurations. In these configurations, the effects of airfoil curvature are considered second-order effects as these sections are relatively short, in the order of less than 0.35 cm (0.138 in.) in a true airfoil scale. The value of the analytical models presented here provides the basis for determining analytically the geometrical effects relevant to each trailing-edge configuration. This analytical approach also offers a platform for benchmarking subsequent experimental testing.

Case 1: Solid Trailing Edge Without Internal Cooling

As way of introduction, a simple wedge model shown in Fig. 3 is considered. In this figure, the airfoil trailing edge is represented by a wedge-fin type of configuration without internal convective cooling. Different cooling schemes will be considered in subsequent models.

If an infinitesimal control volume of Fig. 3 is considered, the mathematical expression, which physically states that the energy being stored in the control volume is equal to the heat being transferred to the system by external convection, and conducted away from the system by thermal conduction, can be given as follows:

$$\underbrace{-\frac{\partial}{\partial x}\left(-kA\frac{\partial T}{\partial x}\right)\delta x}_{\text{Conduction}}+\underbrace{h_g(T_g-T)P\delta x}_{\text{External Convection}}=\underbrace{\rho Ac\frac{\partial T}{\partial t}\delta x}_{\text{Energy Storage}} \qquad (1)$$

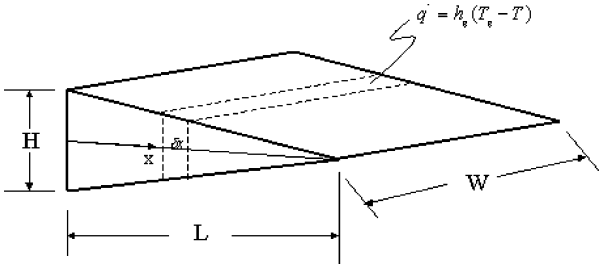

Fig. 3 Trailing-edge analytical model without internal convective cooling.

where

$$A = (HW)[(L-x)/L], \qquad P = 2\{W + H[(L-x)/L]\}u$$

$$u = 2\{1 + [(H/2)/L]^2\}^{\frac{1}{2}}$$

In expression (1), the conduction cross-sectional area A and the corresponding perimeter P of the control volume are functions of the axial distance x. Other geometrical attributes are depicted in Fig. 3. Variables T and T_g denote metal temperature and external gas temperature, respectively. The thermophysical variables k, ρ, c denote the metal thermal conductivity, density, and specific heat capacity properties, respectively. In the right-hand side, time is denoted by variable t. The right-hand-side term of expression (1) will vanish if one considers the steady-state condition only for the control volume. Further, the simplification for large W leads to the following equation:

$$\frac{\mathrm{d}}{\mathrm{d}x}\left[(L-x)\frac{\mathrm{d}T}{\mathrm{d}x}\right]+\left[\left(\frac{h_g}{k}\right)\left(\frac{L}{H}\right)(2u)\right](T_g-T)=0 \qquad (2)$$

Equation (2) is further simplified by a change of variables, using $\theta = T - T_g$ and $y = L - x$, to obtain the fundamental modified Bessel equation of order zero, Eq. (3):

$$y^2\frac{\mathrm{d}^2\theta}{\mathrm{d}y^2}+y\frac{\mathrm{d}\theta}{\mathrm{d}y}-E^2y\theta=0 \qquad (3)$$

where

$$E^2 = [(h_g/k)(L/H)(2u)]$$

To solve this second-order differential equation, two boundary conditions are required. The first boundary condition is located at the base of the wedge model of Fig. 3, at $x = 0$, and requires that $T = T_b$ or $\theta = \theta_b$, where the subscript b stands for a base quantity. The other boundary condition comes from the requirement that the metal temperature at the apex of the wedge model, at $x = L$, be finite. The solution of Eq. (3) then becomes

$$\frac{\theta(x)}{\theta_b}=\frac{I_0\left[2E(L-x)^{\frac{1}{2}}\right]}{I_0\left(2EL^{\frac{1}{2}}\right)} \qquad (4a)$$

or

$$T(x)=T_g-(T_g-T_b)\frac{I_0\left[2E(L-x)^{\frac{1}{2}}\right]}{I_0\left(2EL^{\frac{1}{2}}\right)} \qquad (4b)$$

Solutions (4a) and (4b) are equivalent. Either solution is fundamental in that it assumes a form, which will appear again as the homogeneous solution for problems involving different cooling schemes. These fundamental solutions will always follow the form of solution (4) with different interpretations for the argument E of the Bessel function of second kind and order zero I_0. Variations of the model of Fig. 3 with different internal cooling schemes are now considered.

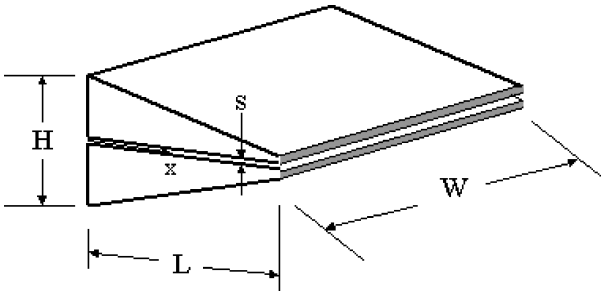

Fig. 4 Trailing-edge model with centerline slot.

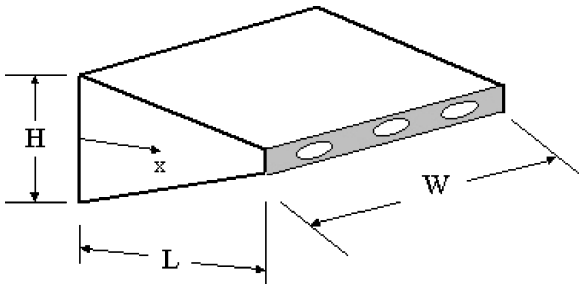

Fig. 5 Trailing-edge model with cooling holes.

Case 2: Trailing Edge with Centerline Slot Discharge

Following the steps outlined earlier for the analysis of the model in Fig. 3, the next model depicted in Fig. 4 is analyzed in similar fashion.

The governing equation is derived as per Eq. (3) with the addition of the nonhomogeneous term S, which accounts for the slot cooling effect. As noted before, the homogeneous solution is provided by Eq. (4). In this case, argument E is modified to account for the internal cooling effect of the centerline slot.

The internal heat-transfer coefficient, denoted by h_c, is assumed constant. In subsequent sections, expressions to relate this internal heat-transfer coefficient to geometrical attributes of the cooling passage will be discussed. Suffice it to say here that the coefficient is considered known and that the sink effect is the particular solution of Eq. (5), defined by the source term S, as follows:

$$y\frac{\mathrm{d}^2\theta}{\mathrm{d}y^2} + \frac{\mathrm{d}\theta}{\mathrm{d}y} - E^2\theta = S \tag{5}$$

where

$$y = L(1 - s/H) - x$$
$$E^2 = (h_g/k)(L/H)(2u) + 2(h_c/k)(L/H)$$
$$S = 2(h_c/k)(L/H)[T_g - T_c(x)]$$

The complete solution of Eq. (5) will be presented in a subsequent section when more details about the coolant temperature distribution are provided.

Case 3: Trailing Edge with Arbitrary Openings in a Centerline Discharge

In the cooling configuration shown in Fig. 5, discrete cooling holes with arbitrary shapes are considered. The formulation follows that performed when the model of Fig. 3 was considered. The resulting governing equation is similar to Eq. (5), with parameters modified to account for the new cooling arrangement.

In this treatment, the geometrical parameter A_H denotes the cross-sectional area of an arbitrarily shaped cooling hole with P_H as the perimeter of the cooling hole.

The term N_H denotes the number of cooling holes in the radial span. The new governing parameters for this configuration become

$$y = L(1 - A_H N_H/WH) - x$$
$$E^2 = (h_g/k)(L/H)(2u) + (P_H N_H/W)(h_c/k)(L/H)$$

and

$$S(x) = (P_H N_H/W)(h_c/k)(L/H)[T_g - T_c(x)]$$

The complete solution of Eq. (5) will be presented in a subsequent section when more details about the coolant temperature distribution are provided.

Case 4: Trailing Edge Cutback Design with Pressure-Side Discharge

This cooling configuration deviates from centerline discharge as the pressure side of the trailing edge has a cutback leading to a pressure-side ejection of the coolant onto the main gas stream. The model shown in Fig. 6 has the trailing edge of the airfoil extended all of the way on the suction (bottom) side with a cutback located on the pressure (top) side. The pressure-side cutback is probably one of the most utilized cooling configurations in today's airfoil design. This permits a significantly thinner trailing edge, approximately 0.76 mm (0.030 in.) vs 1.27 mm (0.050 in.). Therefore, the aerodynamic losses associated with the cutback design attain the lowest values among all of the cases analyzed here.

The governing equation is similar to that given by Eq. (5). For simplicity, the defining governing parameters for this configuration are divided into two parts: one for a side defined up to $x < L_T$ and the other for the suction side defined by $L_T \le x \le L_B$, This leads to

For $x < L_T$:

$$y = \frac{H}{M} - x, \qquad M = \left(\frac{H_T - t_T}{L_T}\right) + \left(\frac{H_B - t_B}{L_B}\right)$$

$$E^2 = \left[\frac{\bar{h}_g(u_T + u_B) - 2h_c}{kM}\right], \qquad S(x) = \left(\frac{2h_c}{kM}\right)[T_g - T_c(x)]$$

with

$$\bar{h}_g = \frac{(h_{g,T} + h_{g,B})}{2}, \qquad u_T = \left[1 + \left(\frac{H_T - t_T}{L_T}\right)^2\right]^{\frac{1}{2}}$$

$$u_B = \left[1 + \left(\frac{H_B - t_B}{L_T}\right)^2\right]^{\frac{1}{2}}$$

and for $L_T \le x \le L_B$:

$$y = \frac{H_B}{M} - x, \qquad M = \left(\frac{H_B - t_B}{L_B}\right)$$

$$E^2 = \left[\frac{h_{g,B}(u_B) - h_c}{kM}\right], \qquad S(x) = \left(\frac{h_c}{kM}\right)[T_g - T_c(x)]$$

For the particular solution of Eq. (5), it is necessary that the term S be obtained. In this case, the external conditions T_g and h_g are

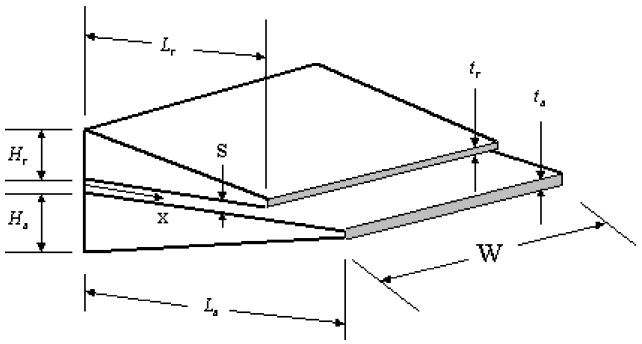

Fig. 6 Cutback trailing-edge model with slots.

assumed known constants for simplicity and convenience, while the coolant temperature T_c needs to be determined.

If one considers a fluid control volume at the same axial distance as that for the control volume shown in Fig. 3, and assuming that the heat flux q'' is a known constant, again for simplicity and convenience, then an expression for the coolant heat pick-up can be written as follows:

$$\rho V A c_P \frac{\mathrm{d}T_C}{\mathrm{d}x}\delta x = q''(x)\delta A_{C,S} \tag{6}$$

where

$$q''(x) = q''_T(x) + q''_B(x) \qquad x < L_T$$
$$q''(x) = q''_B(x) \qquad L_T \le x \le L_B$$

The heat fluxes q''_T and q''_B denote the heat flux from the top and bottom parts of the cooling passage. The quantity $\delta A_{c,s}$ denotes the control volume internal surface area of the cooling passage. The governing Eq. (6) has a single inlet boundary condition at $x = 0$ as $T_c = T_{c,i}$ or $\theta = \theta_{c,i}$, and the solution becomes

$$\theta_c = \theta_{c,i} + \Delta\theta_c(x) \tag{7}$$

where

$$\Delta\theta_c = \frac{q''\Delta A_{C,S}}{\rho V A c_P}$$

Even though the calculation of the trailing-edge metal temperature is an important step in the durability design process, it is equally important to determine the cooling flow rate through the trailing edge. After all, the cooling flow rate is directly related to the internal heat-transfer capability of the cooling design. To estimate the trailing-edge cooling flow, one needs to consider the inlet coolant flow rate, at the root of the supply cavity, denoted here as m_{Root}, as well as the tip-cooling flow rate at the tip, denoted as m_{tip}, and flow variation through the trailing-edge feed cavity. The linear function of cooling flow rate distribution from the root to the tip as flow exits the trailing edge leads to the following flow relationship:

$$m(r) = m_{\mathrm{Root}}(1 - ar) \tag{8}$$

where

$$a = (1/L_H)(1 - m_{\mathrm{Tip}}/m_{\mathrm{Root}})$$

with L_H as the blade span radial height. If there is no communication between the tip holes and the trailing-edge supply cavity, the term a in Eq. (8) is equal to the reciprocal of the blade span radial height, and the trailing-edge flow distribution varies linearly from a finite mass flow rate, at the root section to no-flow condition at the tip.

The temperature of the coolant inside the feed cavity is obtained by considering an infinitesimal small control volume dr in the supply cavity. This consideration leads to the following energy balance:

$$mc_P\frac{\mathrm{d}T_c}{\mathrm{d}r} = \frac{\mathrm{d}Q}{\mathrm{d}r} + \frac{mr\omega^2}{Jg_c} \tag{9}$$

where Q denotes the total heat transfer onto the corresponding trailing-edge section of radial span L_H.

The trailing-edge coolant flow rate of Eq. (8) is then introduced in Eq. (9). The resulting expression is integrated from root to any other radial section of the airfoil. This yields an expression for the coolant temperature increase in terms of heat transfer, and rotational pumping, as a function coolant flow rate. The result is

$$T_c(r) = T_{c,\mathrm{Root}} + \left(\frac{Q_{\mathrm{Total}}}{aL_H m_{\mathrm{Root}} c_p}\right)\ell_n\left(\frac{1 - ar_{\mathrm{Root}}}{1 - ar}\right) + \frac{\left(r^2 - r^2_{\mathrm{Root}}\right)\omega^2}{2Jg_c c_p} \tag{10}$$

This expression allows for calculation of the temperature increase of the coolant in the supply cavity before entering the trailing-edge passages, and it should be used as $T_{c,i}$ for Eq. (7) presented earlier.

Finally, when the particular solution Eq. (7) is substituted in Eq. (5) for evaluating source term S, the following complete solution is obtained:

$$\theta(x) = \frac{I_0\left[2E(L-x)^{\frac{1}{2}}\right]}{I_0\left(2EL^{\frac{1}{2}}\right)}\left[\theta_b - \left(\frac{E_c}{E}\right)^2\theta_{c,i}\right] + \left(\frac{E_c}{E}\right)^2[\theta_{c,i} + \Delta\theta_c(x)] \tag{11a}$$

or

$$T(x) = T_g - \left\{\begin{array}{l}\dfrac{I_0\left[2E(L-x)^{\frac{1}{2}}\right]}{I_0\left(2EL^{\frac{1}{2}}\right)}\left\{[(T_g - T_b] - \left(\dfrac{E_c}{E}\right)^2(T_g - T_{c,i})\right\} \\ \quad + \left(\dfrac{E_c}{E}\right)^2[(T_g - T_{c,i}) + \Delta T_c(x)]\end{array}\right\} \tag{11b}$$

Solutions (8a) and (8b) are equivalent and applicable to all of the configurations studied. The parameters E^2 and E_c^2 for each configuration are summarized in Table 1.

Analytical Solutions and Their Implications on Trailing-Edge Design

To illustrate the realistic characteristics of each design, Table 2 gives representative magnitudes of key variables associated with the parameters listed in Table 1. With these data, the temperature distributions based on Eq. 11(b) for all four configurations are given in Fig. 7. One notable finding is that the solid trailing edge yields the highest metal temperatures approaching 1260°C (2300°F). As per solution (4), using the ratio of Bessel functions requires that the metal temperature profile increase monotonically.

The same trend is observed for the centerline discharge cases of the slot and discrete cooling openings. Based on the input data from Table 2, the maximum temperature occurs at the end of the trailing edge with 1202°C (2196°F) and 1214°C (2219°F) for the slot and discrete cooling openings, respectively. This decrease in metal temperature is a sole function of the sink effect provided by the cooling configuration, as the base temperature and all other conditions are kept constant for all cases considered. One relevant design feature for the centerline discharge configurations is that the cooling design affects the metal temperatures monotonically. That is, if the metal temperature is considered elevated for particular design application, then the only variable to be iterated upon is the coolant passage heat-transfer coefficient to reduce the metal temperature at the end of the trailing edge. Overall this implies

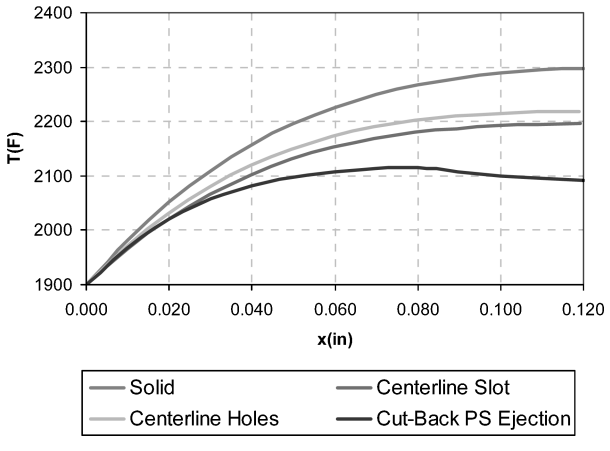

Fig. 7 Metal temperature results for different configuration.

Table 1 Parameters for different models

Configuration	E^2	E_c^2
Solid wedge model (Fig. 2)	$\left[\left(\frac{h_g}{k}\right)\left(\frac{L}{H}\right)(2u)\right]$	0
Wedge with slot cooling (Fig. 3)	$\left(\frac{h_g}{k}\right)\left(\frac{L}{H}\right)(2u)+2\left(\frac{h_c}{k}\right)\left(\frac{L}{H}\right)$	$2\left(\frac{h_c}{k}\right)\left(\frac{L}{H}\right)$
Wedge with cooling holes (Fig. 4)	$\left(\frac{h_g}{k}\right)\left(\frac{L}{H}\right)(2u)+\left(\frac{A_{S,H}N_H}{W}\right)\left(\frac{h_c}{k}\right)\left(\frac{L}{H}\right)$	$\left(\frac{A_{S,H}N_H}{W}\right)\left(\frac{h_c}{k}\right)\left(\frac{L}{H}\right)$
Cutback wedge with slot cooling (Fig. 5)	$\left[\frac{\bar{h}_g(u_T+u_B)-2h_c}{kM}\right]$ for $x<L_T$	$\left(\frac{2h_c}{kM}\right)$ for $x<L_T$
	$\left[\frac{h_{g,B}(u_B)-h_c}{kM}\right]$ for $L_T\le x\le L_B$	$\left(\frac{h_c}{kM}\right)$ for $L_T\le x\le L_B$

Table 2 Boundary conditions for trailing-edge examples[a]

Configuration	Solid	Centerline slot	Centerline holes	Cutback PS ejection
Figure	2	3	4	5
T_g	2300	2300	2300	2300
$\Delta T_{c,T}$, ΔT_c	50	50	50	50
$\Delta T_{c,B}$	——	——	——	150
$T_{c,\text{in}}$	1600	1600	1600	1600
T_{base}	1900	1900	1900	1900
h_g or $h_{g,T}$[b]	2000	2000	2000	2000
$h_{g,B}$[b]	——	——	——	1000
h_c[b]	2000	2000	2000	——
$h_{c,T}$[b]	——	——	——	2000
$h_{c,B}$[b]	——	——	——	2500
k[c]	12	12	12	12
L_T or L	0.12	0.12	0.12	0.08
L_B	——	——	——	0.12
H_T or H	0.06	0.06	0.06	0.03
H_B	——	——	——	0.03
t_T	——	——	——	0.01
t_B	——	——	——	0.029
P_H	——	0.05	——	——
d_h	——	——	0.015	——
W	——	——	2.5	——
S	——	0.015	——	0.015

[a]All length dimensions in inches and temperatures in degrees Fahreinheit. 1 in. = 0.0254 m; $F = 32 + (\frac{9}{5})$ C.
[b]h_c, h_g = BTU/(hr-ft^2-F).
[c]k = BTU/(hr-ft-F); BTU/(hr-ft^2-F) = 5.68 W/(m^{2}K); BTU/(hr-ft-F) = 1.73 W/(m K).

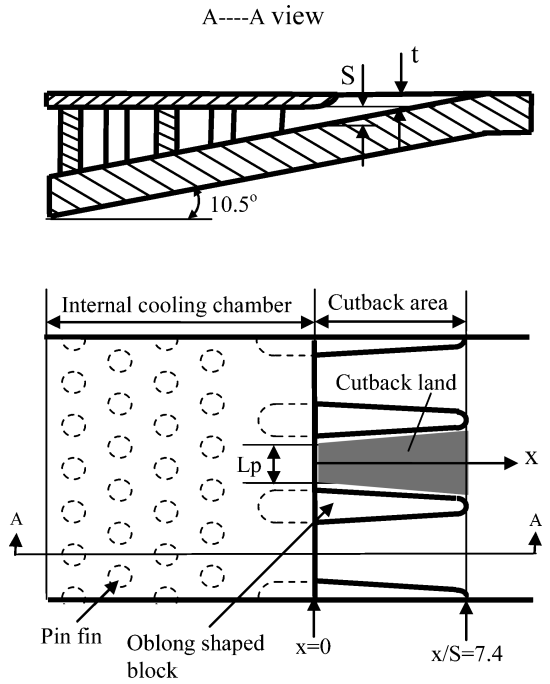

Fig. 8 Schematics of the trailing-edge configuration.

that either the size of the coolant passage need to be increased, or the features inside the passage need to be modified to enhance the magnitudes of internal heat-transfer coefficient. Alternatively, higher coolant flow rates can be increased to enhance cooling. This approach is viable only if sufficient supply pressure is available.

For the configuration with a pressure-side ejection cutback trailing edge, the limitations associated with the thicker trailing edge of the centerline designs are removed. As shown in Fig. 7, the metal temperature profile does not increase monotonically for pressure-side ejection designs. This allows for several alternative design options to optimize the cooling configuration. These are 1) size of the cooling passage can be increased; 2) internal cooling features inside the cooling passage could be selected to enhance internal heat transfer; 3) trailing-edge thickness could be made thinner; 4) pressure-side lip thickness could be made thinner; 5) pressure-side land roughness could be increased to augment coolant heat transfer; and 6) slot film effectiveness could be increased with higher coverage. From this set of design features, only two features, namely, 1 and 2, can be used realistically for centerline discharge designs, whereas all features, 1 through 6, can be used for pressure-side ejection cutback trailing-edge designs. There are also benefits of improved aerodynamic performance with a thinner trailing edge. In addition, the thermal-mechanical fatigue and creep life capability are also improved as metal temperature distributions are improved for the entire trailing-edge region of the airfoil.

Experimental Setup and Procedures

In this section, the experimental procedure uses a hybrid measurement technique based on transient liquid crystal imaging. The hybrid denomination is based on two different test procedures: 1) the one-dimensional transient model for surface uncovered by pedestals and 2) one-lumped heat-capacity model for the heat transfer over pedestal surfaces. Both of these models will be discussed in detail in this section. The hybrid technique employs the transient conduction model in a semi-infinite solid and the lumped capacitance method for resolving the heat-transfer coefficient for the end-wall surface uncovered by the pedestals and for the pedestal surface, respectively. A brief description of the hybrid method and data reduction is also presented in this section.

The test section is a scaled-up model, made of Plexiglas® of the actual trailing edge. Figure 8 is a schematic view of the configuration. The internal cooling chamber is a convergent wedge-shaped duct, with four-row staggered pin fin arrays. Near the exit of the duct, oblong-shaped features are used for connecting the pressure side and the suction side. All pedestals or pins are positioned orthogonally relative to the mainstream. The suction-side wall has 10.5-deg

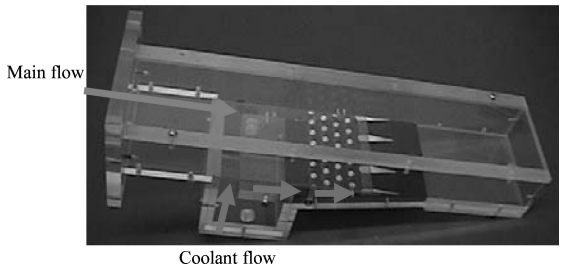

Fig. 9 Photo of the trailing-edge test rig.

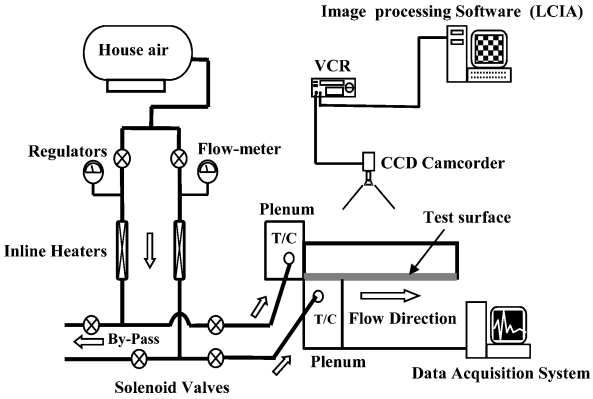

Fig. 10 Test apparatus.

inclination relative to the horizontal line, as shown in Fig. 8. The pin diameter is $d = 6.0$ mm. The pin spacing along the longitude and transverse direction is the same, that is, $s_l/d = s_p/d = 2.0$. The pins and the oblong-shaped features are made of aluminum, which has high thermal conductivity for the lumped-capacity model. On the other hand, the surfaces modeling the pressure and suction sidewalls are made of Plexiglas, the low thermal conductivity of which is required for the use of transient semi-infinite solid conduction model. The pressure-side cutback area partitioned by the oblong-shaped features is also shown in Fig. 8. The land section subjected to film-cooling measurement is highlighted in blue color for reference.

Figure 9 shows a photo of the actual test rig. The rig, made of Plexiglas, is of rectangular cross section, 38.1 mm (1.5 in.) high and 76 mm (3 in.) wide. To model the film-cooling situation, mainstream is provided outside the pressure side. The coolant enters through a settling chamber underneath the test rig, then turns rightward to the pedestal cooling channel and injects on the cutback land. For the internal heat-transfer study, the main flow is not introduced.

The test surface is coated with a thin layer of thermochromic liquid crystal (TLC) about 0.1 to 0.3 mm (0.004 to 0.012 in.) thick. An airbrush is used to spray coating. The temperature calibrated for the particular TLC used in the present study is 36°C (96.8°F) for the maximum green color intensity. The maximum green intensity displayed by TLC is used as the surface temperature tracer during a transient measurement. Figure 10 shows a schematic of the test setup. A laboratory compressor supplies both the main stream and film-cooling flows. Flow rates of the compressed air are measured by standard American Society of Mechanical Engineers orifices. After metered, each stream is routed through a tubular in-line heater controlled by an autotransformer, and its temperature can be accurately set to a desired level. Downstream of the heater, two flows are initially diverted away from the test section by a three-way ball valve before starting the test.

Before starting the test, the flows are diverted to bypass so that the test section remains at the laboratory ambient temperature. When the flow rate and the temperature have reached steady state, the valves are suddenly switched to introduce the flows to the test section. Initiation of the test also triggers an automated data-acquisition system for recording thermocouple readings at flow inlet and as well as exit. Simultaneously, a charge-coupled-device camera starts to record the video images of the TLC coated on the test surface. The video provides the follow-on data-reduction procedure with the lap time of TLC changing from colorless to green at every pixel of the viewing domain. The postrun data-reduction procedure uses a custom-developed software in a personal computer to get the local heat-transfer coefficient.[25] As mentioned before, only the film-cooling flow line is used, with main flow line closed, for the internal cooling chamber heat-transfer tests; otherwise, the experimental procedure is basically the same as that in the preceding description.

Hybrid Method and Data Reduction

For internal cooling chamber, the local heat-transfer coefficient over the uncovered end-wall surface is obtained by using one-dimensional transient conduction over a semi-infinite solid, while the regional-averaged heat-transfer coefficient over the pin surface is resolved by using the lumped-capacity model. The following are brief introductions of both approaches.

One-Dimensional Transient Model

The one-dimensional transient model treats the substrate beneath the surface as a semi-infinite solid domain, as illustrated in Fig. 11. When the surface is suddenly exposed to a forced flow stream, with a steady convective heat-transfer coefficient h, prescribed on the surface, the temperature field in the solid domain can be modeled by the following one-dimensional, transient heat-conduction equation, that is,

$$k\frac{\partial^2 T}{\partial z^2} = \rho c\frac{\partial T}{\partial t} \tag{12}$$

with boundary and initial conditions

$$-k\left.\frac{\partial T}{\partial z}\right|_{z=0} = h(T_w - T_r) \tag{13}$$

$$T|_{z=\infty} = T_i \tag{14}$$

$$T|_{t=0} = T_i \tag{15}$$

where T_i is the initial temperature of the test section, T_w is the local surface temperature, and T_r is the flow reference temperature. The difference between the temperatures T_w and T_r represents the driving potential for the convective heat transfer in the system. Equations (12–15) lead to a solution of T_w expressed as

$$(T_w - T_i)/(T_r - T_i) = 1 - \exp[h^2\alpha t/k^2]erfc\left[h\sqrt{\alpha t}\Big/k\right] \tag{16}$$

The reference temperature T_r is equal to the temperature of the hot air or flow bulk. As the time-varying TLC images can provide a relation between temperature T_w and time t over the entire viewing domain, the distribution of local heat-transfer coefficient h can be resolved from the preceding equation.

In an actual experiment, a perfect step change of the applied flow temperature is usually not possible, and the reference temperature, in fact, is a function of time. This can be accounted for by modifying the solutions via superposition and Duhamel's theorem. The solution becomes

$$T - T_i = \sum_{i=1}^{N} U(t - \tau_i)\Delta T_r \tag{17}$$

where

$$U(t - \tau_i) = 1 - \exp[(h^2/k^2)\alpha(t - \tau_i)]erfc\left[(h\Big/k)\sqrt{\alpha(t - \tau_i)}\right] \tag{18}$$

with

$$\alpha = k/\rho c$$

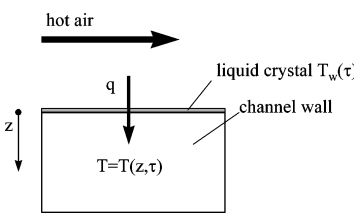

Fig. 11 Schematic of one-dimensional transient heat transfer model.

The local heat-transfer coefficient on the uncovered end wall is obtained by using the preceding two equations (17) and (18).

Lumped-Heat-Capacity Model

Consider a test element with a mass m and initial temperature T_i that is suddenly exposed to a flow stream that has a steady temperature T_r and imposes a convective heat-transfer coefficient h on the element's surface. If the element is of low Biot number, its temperature as function of time $T(t)$ can be modeled by an initial value problem, that is,

$$hA(T - T_r) = -mc\frac{\mathrm{d}T}{\mathrm{d}t} \tag{19}$$

and

$$T|_{t=0} = T_i \tag{20}$$

where A is the effective heat-transfer area and c is the heat capacitance of the element. The solution to the preceding equation is

$$(T - T_i)/(T_r - T_i) = 1 - \exp(-hAt/mc) \tag{21}$$

For imperfect step changes in flow temperature, superposition and Duhamel's theorem are applied, as in Eqs. (17) and (18). In present study, the regional-averaged heat-transfer coefficient over the pedestal surface is resolved by using this method.

As for the test method and data reduction for the film-cooling study, basically, two tests, called "hot test and cold test," are needed, and two coupled equations similar to Eq. (14) are solved to obtain film-cooling effectiveness and heat-transfer coefficient h. Detailed information can be found in Ref. 23.

Governing Parameter Definitions

For the internal cooling chamber investigation, the channel is convergent channel, and, as a result, the flow area along the flow direction is changing. Therefore we set the minimum area A min, as the first row of pins is used for Reynolds-number definition,

$$Re = \rho Qd/A\min\mu \tag{22}$$

where Q is the volume flow rate and d is the diameter of the circular pin. For Nusselt number, pin fin diameter d is used as characteristic length, yielding the definition

$$Nu = hd/k \tag{23}$$

For the film-cooling performance on cutback land study, the definition of blowing ratio is given as follows:

$$M = (\rho U)_f/(\rho U)_m \tag{24}$$

where subscripts m and f represent main flow and film cooling, respectively. The density ratio in the present study is equal to one. Hence the existing blowing ratio is essentially the flow velocity ratio between the film-cooling flow and the main flow. The Reynolds numbers for main flow and film-cooling flow are defined as

$$Re_m = \rho UD_h/\mu \tag{25}$$

and

$$Re_f = \rho MUd_h/\mu \tag{26}$$

where D_h is the hydraulic diameter of the rectangular duct and d_h is the hydraulic diameter of film-cooling injection slot. For the present configuration, its value is calculated from the cross-section area at the exit of the internal cooling chamber. The variable U denotes the mean velocity of main flow.

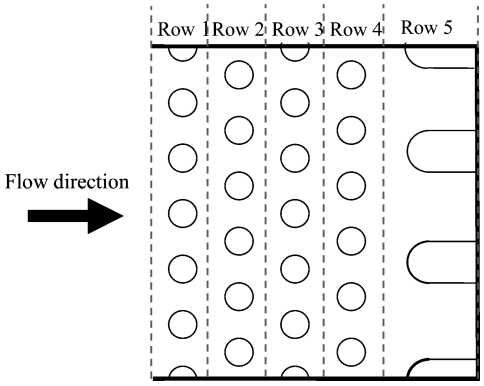

Fig. 12 Covered area for each row.

Results and Discussion

Heat Transfer in Internal Cooling Chamber

The heat transfer in such a cooling configuration combines the effect of flow acceleration as a result of gradually decreasing cross-section area and pin fin effects with varying height. Thus, the heat-transfer values could be very different from the results obtained from either the general pin fin or smooth wedge-shaped duct heat-transfer study. Five cases with different Reynolds number ranging from 3.5 to 9.5×10^3 have been tested. The results are also compared directly to those of pin fin studied earlier by Chyu.[25] The value of the Nusselt number Nu is estimated to have an uncertainty of less than $\pm 7\%$ based on an uncertainty analysis technique developed by Kline and Mclintock.[26]

The heat-transfer coefficients are to be presented in respect of the row average for pin, end wall, and both combined. Each row covered heat-transfer area is illustrated in Fig. 12. In particular, the end-wall area of each row is the area covered by that row subtracting the area occupied by pins or shaped blocks in the row.

The overall averaged Nusselt number for each row or entire wetted surface domain is obtained by employing the formula in the form of

$$Nu = \frac{Nu_{\text{endwall}} \times A_{\text{endwall}} + Nu_{\text{pin}} \times A_{\text{pin}}}{A_{\text{endwall}} + A_{\text{pin}}} \tag{27}$$

where A_{pin} represents the effective heat-transfer area of the pin fin surface. Because both ends of a fin element are attached to the end wall, the effective heat-transfer area is only the circumferential area of the fin element, that is,

$$A_{\text{pin}} = n \cdot \pi \cdot d_{\text{pin}} \cdot H \tag{28}$$

To demonstrate the heat-transfer enhancement effect, the Nusselt number is normalized by the corresponding Nusselt number of a smooth duct Nu_0 at the corresponding Reynolds number Re_0.

End-Wall and Pin-Averaged Heat-Transfer Coefficient

Figure 13 presents the end-wall and pin-averaged heat-transfer coefficient of each row for five different Reynolds numbers. One noticeable feature revealed in the figure is the increase of the averaged heat-transfer coefficient, which reaches its maximum at the fourth row. This is consistent with the result of previous general pin fin heat-transfer studies. Because the fifth row of pin has different configuration and geometrical arrangement, the heat-transfer coefficient shows a decrement ranging from 9 to 43% compared to that of the fourth row. The mechanism for this significant drop of the heat-transfer coefficient can come from two aspects. On the one hand, the increase of the heat-transfer coefficient is minor, or nonexistence, after the fourth row of pin. On the other hand, the flow velocity after the fourth row of pins tends to decelerate as a result of the enlarged free spacing. This can significantly reduce the turbulence and thus affect the heat transfer in the fifth row.

Another feature revealed from Fig. 13 is the higher average heat-transfer coefficient of the end-wall area compared to that of

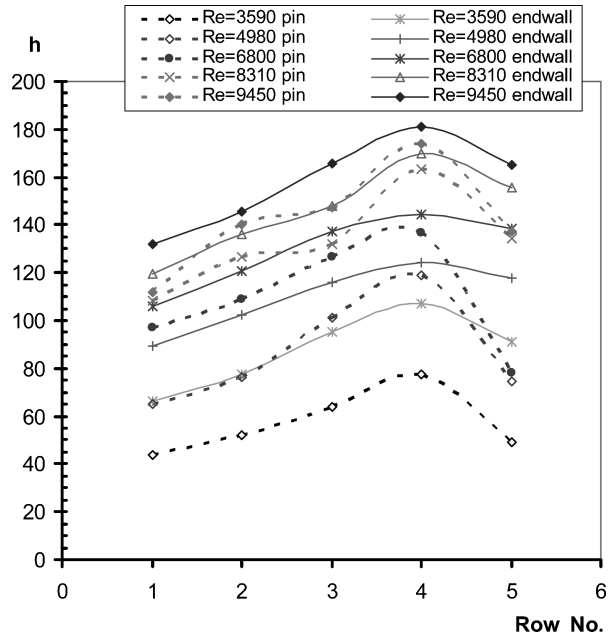

Fig. 13 Row-averaged heat-transfer coefficient.

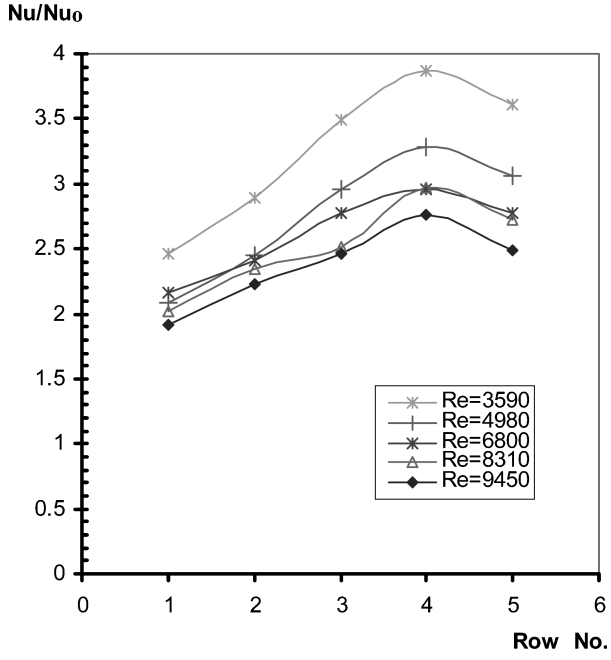

Fig. 14 *Nu/Nu*$_0$ value by row.

the pins. It might be easy to understand that the contracting feature of the channel in the present configuration allows the pin-generated turbulence to have a stronger effect to the end-wall heat transfer.

Row-Averaged Nusselt Number

Illustrated in Fig. 14 is the row overall averaged Nusselt number normalized by Nu_0 for each row at the five tested Reynolds numbers. All rows have some extent of heat-transfer enhancement, in the ratio of Nu/Nu_0 ranging from 1.9 to 3.9. The magnitude of heat-transfer enhancement gradually increases from the first row to the fourth row, which agrees well with the trends of the variation of the row averaged pin and endwall heat-transfer coefficient. The fifth row has the same level of heat-transfer enhancement as that of row 3, though there is a decrease relative to the fourth row.

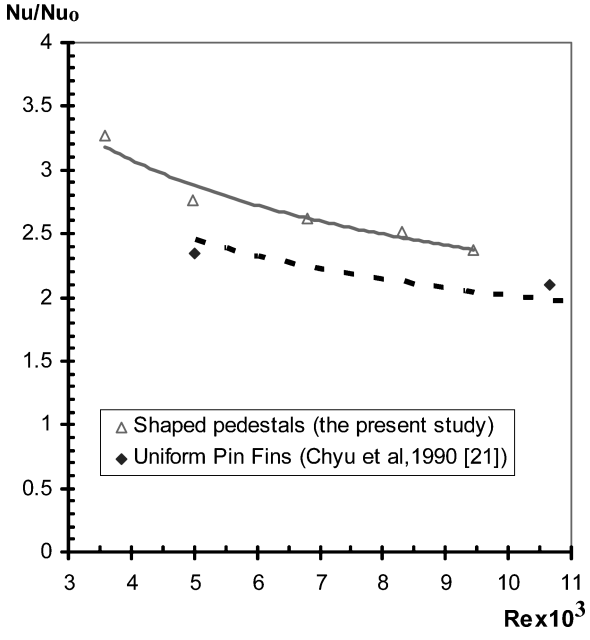

Fig. 15 Comparison of heat-transfer enhancement.

Area-Averaged Nusselt Number

The entire domain averaged Nusselt-number values for all of the tested Reynolds numbers are also normalized by Nu_0. Nu/Nu_0 vs Re is plotted in Fig. 15 to show the effect of Reynolds number on the level of heat-transfer enhancement. The magnitude of Nu/Nu_0 decreases exponentially with the Reynolds number, which is similar to typical cases involving turbulent flow impingement and separation.

Also plotted together are the results of uniform pin fins[25] for comparison. The value of the enhancement for the present configuration ranges from 2.4 to 3.3 for all tested Reynolds number. The enhancement is comparable to that of uniform pin fin structure, with at least 10% higher than those of uniform pin fin structure at the tested Reynolds numbers.

Film-Cooling Performance on Cutback Land

The film-cooling performance over the cutback land is expected to be different from that in the case of clear slot as the internal cooling chamber structure significantly affects the coolant flow. By introducing elements inside, the present studied configuration generates strong turbulence for the coolant flow before it injects from the exit of slot. In addition, the oblong-shaped features, laterally interrupting the cutback region, make the main flow three dimensional. Such a complicated interaction between the turbulent coolant flow and the three-dimensional main flow could be very detrimental to the film cooling on the cutback land. To examine the film-cooling performance on the cutback land of this configuration, four blowing ratios ($M = 0.7$, 1.0, 1.32, and 1.96), with fixed main flow Reynolds number $Re_m = 3.74 \times 10^4$ and corresponding coolant flow Reynolds number $Re_f = 3.03$, 4.25, 5.76, and 8.34×10^3, were tested. The geometrical parameters used in the result presentation are illustrated in Fig. 8.

Local Film-Cooling Effectiveness

Figure 16 presents the local film-cooling effectiveness over the cutback land. As expected, the film effectiveness increases with blowing ratios.

Spanwise-Averaged Film-Cooling Effectiveness and Heat-Transfer Coefficient

Figures 17 and 18 shows the spanwise-averaged film-cooling effectiveness and heat-transfer coefficient, respectively. For all tested blowing ratios, the film-cooling effectiveness decreases monotonically as x/s increases. Value of the film effectiveness is above 0.4 for $x/s < 7.4$, which is the length of the cutback land.

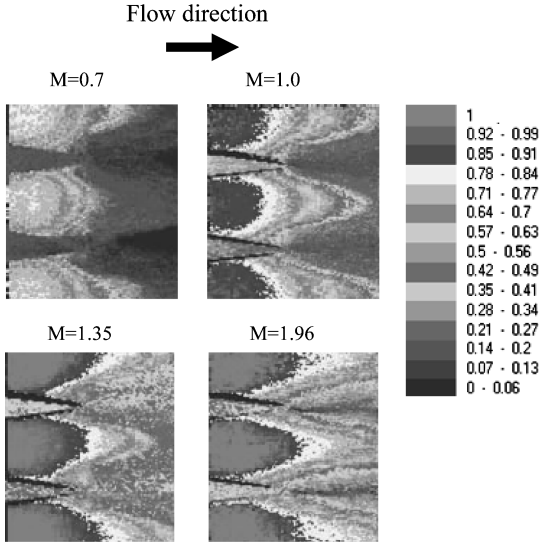

Fig. 16 Local film-cooling effectiveness distribution.

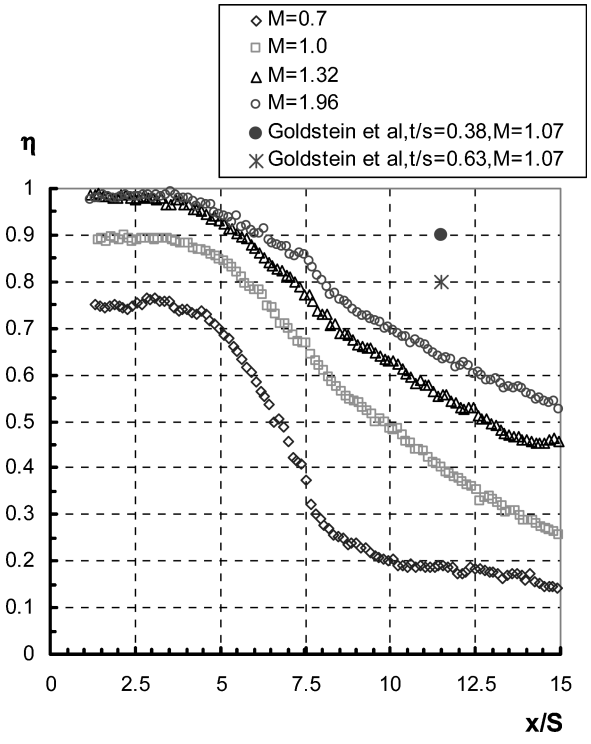

Fig. 17 Spanwise-averaged film-cooling effectiveness.

The ratio of lip thickness t to slot height s for the present configuration is $t/s = 0.432$. For comparison purposes, the results of close t/s ratios in Goldstein's study[27] for clear, two-dimensional slot-injection film cooling are plotted together. As shown in Fig. 17, the film-cooling effectiveness for the current configuration at $x/s = 11.5$, which is already out of the actual trailing-edge end (where $x/s = 7.4$), is much lower than that in clear slot case. The turbulence of the coolant flow caused by the pedestals inside the cooling chamber probably attributes to this decreasing value.[13,15]

As shown in Fig. 18, typically, the value of h is relatively low immediately downstream to the slot injection, rises to a local maximum at x/s around 7.5, and then decreases rapidly downstream. Starting from x/s about 9, it has a relative stable value. Geometrically, the lip affects the location where a shear layer is formed by two separated emerging streams. Similar to the situation of flow over a backward-facing step, the turbulence and mixing level in the region directly beneath the shear layer, or immediately behind the step, are relatively low. This, in turn, results in a low heat-transfer coefficient. As the width of shear layer expands and eventually lands on surface downstream, the magnitude of heat transfer is expected to reach a maximum because of the reattachment effect. Further downstream, the magnitude of the heat-transfer coefficient decreases as the boundary layer grows thicker.

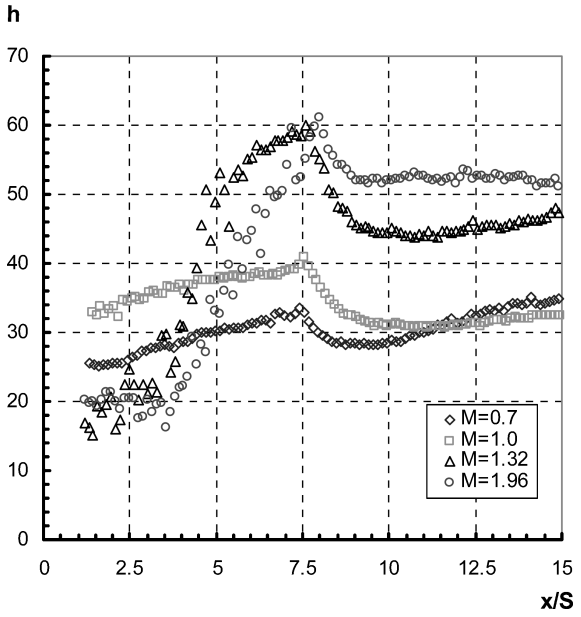

Fig. 18 Spanwise-averaged heat-transfer coefficient.

Heat Transfer Relative to Uncooled Situation

The wall heat-transfer rate per unit area, that is, heat flux, with film cooling can be determined by

$$q = h(T_{\text{aw}} - T_w) \tag{29}$$

where T_{aw}, the adiabatic wall temperature, is related to the film effectiveness via the definition of $\eta = T_{\text{aw}} - T_m / T_f - T_m$. According to Metzger et al.,[28] Sen et al.,[29] and Ekkad et al.,[21,22] the ratio of heat flux on a film-protected surface to the corresponding baseline value without film cooling q_0 can be expressed as

$$q/q_0 = (h/h_0)(1 - \eta/\varphi) \tag{30}$$

where φ is the overall cooling effectiveness given by $\varphi = (T_w - T_m)/(T_f - T_m)$. For any effective film protection, the value of q/q_0 should be less than one. The situation when $q/q_0 = 0$ represents a limiting case that the local surface is fully protected by the cooling film. While the typical values of φ ranges from 0.5 to 0.8 (Ref. 23) in the main-body section. The value of $\varphi = 0.8$ was assumed more appropriate for this work and is used in the calculation of the present evaluation.

The q/q_0 values are plotted in Fig. 19. For all tested blowing ratios, the magnitude of q/q_0 is less than 15% for $x/s < 7.5$. Particularly for $M > 1.32$, the protection is very effective for $x/s < 7.5$, as $q/q_0 = 0$. A noticeable feature revealed in the plots is that for $M = 0.7$, q/q_0 has a relative high value for $x/s < 2.6$. This phenomenon might result from the nonuniform coolant distribution as the blowing ratio is relatively small.

Cooling Considerations in Trailing-Edge Design

Combined Centerline Discharge and Pressure-Side Cutback

Cooling high-pressure turbine airfoils are cooled internally with compressor air that enters a blade inlet plenum just before flowing into the blade internal cavities. However, some designs can use cooling media other than air. For instance, in closed-loop cooling

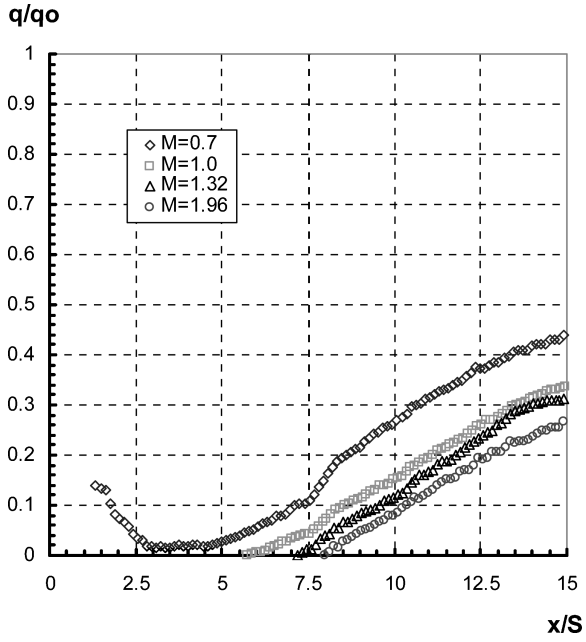

Fig. 19 Spanwise-averaged q/q_0.

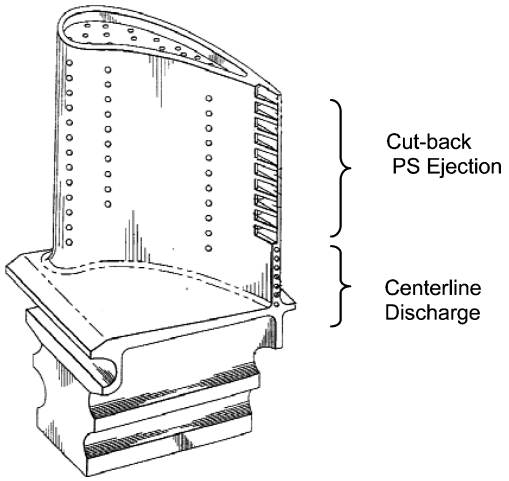

Fig. 20 Typical high-pressure turbine blade showing trailing-edge cooling openings and pressure-side ejection slots, from Lee.[32]

combined-cycle powerplants, the cooling medium is steam.[30,31] Regardless of the cooling medium, the overall design procedures that govern the airfoil trailing-edge cooling remain the same.

To illustrate various facets of trailing-edge design, this part of discussion begins by considering a typical high-pressure turbine-blade configuration from Lee,[32] shown in Fig. 20. Air enters an inlet plenum located underneath the blade. Cooling air passes onto the blade as rotating forces pump the flow towards blade internal cavities and eventually to the trailing edge. In the embodiment of Fig. 20, the trailing-edge configuration is made up of two cooling arrangements: 1) the pressure-side cutback with slots, located in the upper portion of the blade, and 2) the centerline discharge with round openings located in the lower portion of the blade. The combination of these two trailing-edge cooling schemes in one component is the essence of this design. In line with the material presented in the preceding sections, the combination of slots and round openings at the trailing edge provides a performance improvement caused by the thin trailing edge in the upper portion of the airfoil.

The use of centerline discharge with cooling holes in the lower portion of the blade is practical, as the gas-path temperatures can be considerably reduced at the lower radial portion of the airfoil. This effect is aided by hot gas-path migration to the blade tip and stage profile attenuation. The advantage of a thicker trailing edge at the lower portions of the blade stems from the structural requirements. In general, high centrifugal stresses exist in the lower regions, and it might be necessary to add material to the blade at the trailing edge to, among other considerations, decelerate the thermal response of the airfoil trailing edge relative to the rest of the airfoil and end walls. In this way, both creep and thermal-mechanical material fatigue resistance can be increased. Thus, it should be recognized that a combination of trailing cooling schemes can provide preferred arrangements for specific designs, as suggested here for the model of Fig. 20. However, there are many other trailing-edge design configurations in operation today as listed in Refs. 30–39.

Internal Cooling near Trailing Edge

In an attempt to describe other relevant details associated with trailing-edge design, attention is given to the design depicted in Fig. 21, from Hill et al.[40]

This figure illustrates a cross-sectional area of a typical high-pressure turbine blade. It is observed from this cross section that there exists a supply cavity that provides cooling air through a series of impingement crossover holes. The cooling circuit ends at the trailing-edge pressure-side slots in a cutback arrangement.

In Fig. 20, tip pressure-side film holes are in communication with the trailing-edge supply cavity. Tip cooling is done through film-cooling holes located close to the blade tip. Even though the function of these tip holes is to cool the blade tip with air film, preventing tip oxidation, it reduces the flow to the trailing edge. Clearly, such flow interaction is accounted for during trailing-edge cooling requirements as previously expressed by Eq. (11).

Inside the trailing-edge internal cavities, a large number of cooling features can be explored in the design space to enhance internal cooling. For instance, internal trailing-edge cooling configurations can consist of more than one set of impingement rows with internal cooling features, such as pedestals and/or trip strips or turbulators.

Impingement cooling configurations have been used extensively in the gas-turbine blades. In general, cooling air is allowed to pass through crossover openings (i.e, circular holes, racetrack holes, elliptical holes, or slots) leading to jet impingement on the downstream airfoil ribs and surrounding walls. In these designs, coolant flow acceleration is high through crossover impingement openings. As a result, coolant flow Mach-number profiles, which are related to the coolant local static pressure, almost always assume nonuniform, or stepwise characteristics, as the coolant flow crosses these openings. Stepwise or nonuniform coolant profiles are undesirable as they lead to spatial nonuniformity in internal heat-transfer coefficients at the walls of the blade. Such nonuniformity is evident in a recent study by Chyu et al.,[15] as shown in Fig. 22.

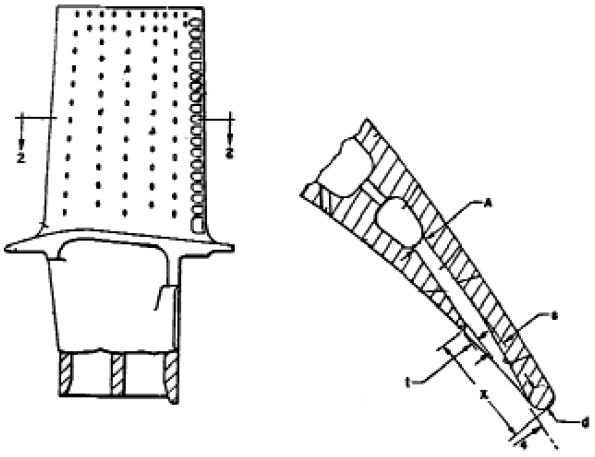

Fig. 21 Typical high-pressure turbine blade showing cross-sectional area and trailing-edge detail, from Hill et al.[40]

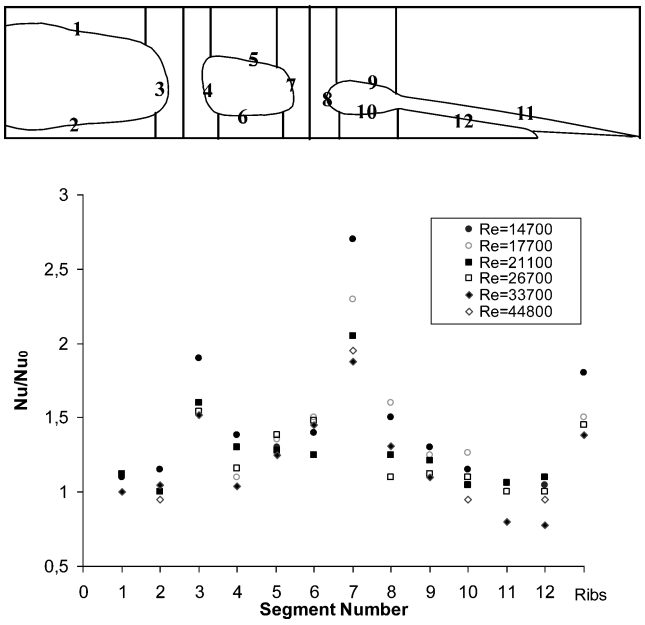

Fig. 22 Localized heat-transfer enhancement on different segments in trailing-edge cavities, from Chyu et al.[15]

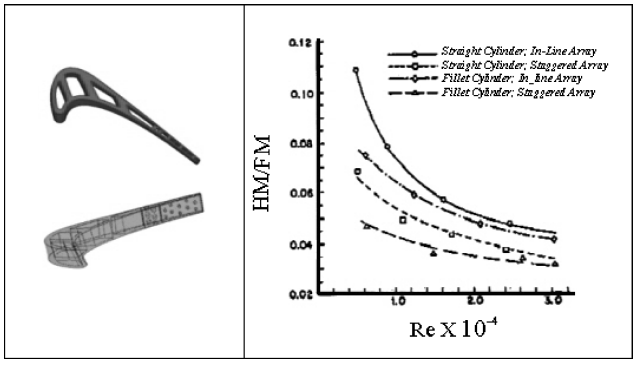

a) b)

Fig. 23 Pedestal trailing-edge configuration and test results: a) transparent view of blade showing pedestal bank at trailing edge and b) effect of Reynolds number on performance index (HM/FM) in straight pins with fillets, from Chyu.[25]

Segment number 7, which is subjected to direct impingement of the accelerated flow exited from the first set of crossover holes, experiences the highest overall heat transfer, nearly three to four times the Nu/Nu_0 of those surfaces without direct impingement. This overall implies that there are regions in the blade walls, which attain relative lower metal temperatures caused by high internal heat-transfer coefficients. Meanwhile, other areas can attain relatively higher metal temperatures caused by lower internal heat-transfer coefficients. Thus, stepwise profiles of coolant jets could lead to stepwise metal temperature differences, which, in turn, can lead to high thermal strains. In parallel to these temperature and heat-transfer differences, relatively fast blade trailing-edge thermal response during takeoff or power loading can exacerbate further undesirable thermal-mechanical effects of metal fatigue at the airfoil trailing edge.

It is therefore necessary to design a trailing-edge cooling configuration that improves the internal profiles for Mach number, static pressure, and internal heat-transfer coefficient distributions. In this regard, internal features, such as pedestals, provide distinct advantages. Optimal designs can include internal pedestals with many different cross-sectional areas, such as circular, oval, racetrack, square, rectangular, diamond, clover-leaf cross sections, just to mention a few. In this context, Zukauskas[41] has suggested how the Reynolds number, based on pin or pedestal diameter, can be used to characterize the flow passing through the trailing-edge internal chambers in terms of corresponding Nusselt numbers for assessing the internal heat-transfer capability. However, certain correction measure is needed here, as Zukausas's correlations are primarily for two-dimensional tube bundles and without taking account of pin-end-wall interaction. The corresponding internal heat-transfer enhancement or heat multiplier, HM, is then normalized by the smooth channel Dittus–Boelter correlation to assess the effectiveness of the cooling design. Similarly, in this context, the pressure drops through a bank of pedestals, lead to the notion of the friction multiplier, FM, normalized with Blasius resistance formula from the experimental results of Ishida and Hamabe.[42]

The corresponding relationships provided by Refs. 41 and 42 for the heat and friction multipliers, HM and FM, can fully characterize the trailing-edge cooling design with pin fins, in terms of cooling effectiveness. The spacing and location of these internal cooling features are then optimized to ensure the elimination of stepwise distributions of metal temperatures in the airfoil trailing-edge walls. These features are presented here as representations of typical design procedure; however, there are many other features or combination of features that could be used effectively as well. In all design cases, experimental correlations are needed to assess a multitude of cooling feature characteristics. Some of these correlations are compiled by Han et al.[43]

The overall procedure for designing airfoil trailing edges with optimum heat-transfer characteristics relies on the knowledge of the corresponding heat and friction multipliers, HM and FM. In many instances, plots of FM/HM vs Reynolds number are used to compare the performance of different configurations. One such plot is shown in Fig. 23, based on mass-transfer measurements conducted by Chyu.[25] Using a well-established analogy between heat transfer and mass transfer,[44] the results of these experiments for different cooling features can be used to assess heat transfer characteristics of the overall cooling design. Information as such, also known as performance index, is useful in the design process as they relate heat-transfer characteristics of different cooling features with available pressure gradients and flow requirements.

External Cooling near Trailing Edge

In conjunction with the internal heat transfer, the heat-transfer characteristics on external airfoil surface near the trailing edge also need to be evaluated in detail. As mentioned earlier, the performance of the airfoil is affected considerably by the thickness of the trailing edge. It is, therefore, necessary to have an airfoil trailing edge with minimum thickness and with a cooling configuration that allows for lower coolant flow rate while not exceeding the metal temperatures required for the metal durability in terms of oxidation, creep, and fatigue. Meanwhile, one would like to have cast-in features as much as possible to avoid machining cost and process time.

In examining possibilities for film cooling for the design of Fig. 21, one recognizes that the airfoil has trailing-edge cavities and slots in communication with the supply cavity. The slot outlet is disposed at a cutback downstream edge of the pressure side wall with a thickness t. A number of channels with width s at the slot outlet allows for discharge cooling air over the extended backsurface suction side wall or the so-called land. If a film-cooling parameter P is defined as a dimensionless airflow parameter directly proportional to the cutback distance x and inversely proportional to the slot s and the cooling flow rate ratio, one obtains the relation $P = x/(Ms)$ with M being the blowing parameter defined as the ratio of coolant to gas mass flux ratio, $M = (\rho_c v_c) / (\rho_g v_g)$. This film-cooling parameter P is critical in film effectiveness calculations, as it has been used to correlate the film-cooling effectiveness η_F at the trailing edge as shown in Fig. 24.

Higher values of the film-cooling parameter P imply greater cutback distances and less airflow for an equivalent film-cooling effectiveness η_F. It has been recognized that high film effectiveness can be maintained over significantly longer cutback distances with less air if the ratio t/s is low.[40] According to Fig. 24, the value of η_F can remain constant as x increases, if the value of the ratio t/s

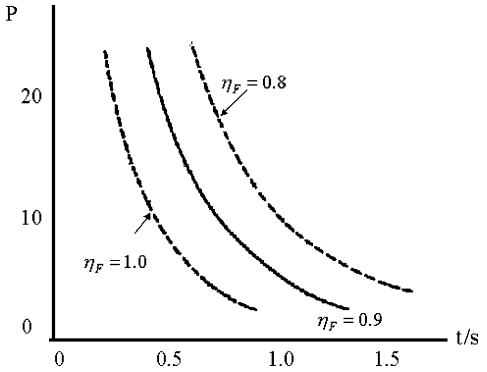

Fig. 24 Dimensionless flow parameter *P* as function of ratio of cutback lip thickness to slot for different film-cooling effectiveness, from Hill et al.[40]

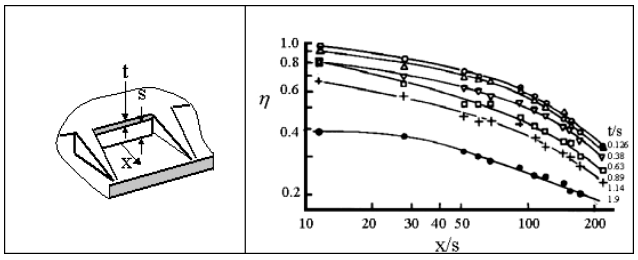

a) **b)**

Fig. 25 Cutback trailing-edge configuration and test results: a) schematic showing locations of relevant geometrical parameters and b) effect of *x/s* and *t/s* parameters on trailing-edge film effectiveness, from Goldstein.[27]

is decreased. This implies that if all other parameters affecting P are held constant the cutback distance x could be increased significantly without loss of film-cooling effectiveness over the length of the cutback portion, if the ratio t/s is decreased. Alternatively, or in combination, the coolant flow rate could be reduced and the cutback distance increased. In this context, Goldstein[27] also presented experimental results for film effectiveness of various t/s ratios and the blowing parameter M of unity. These results are shown in Fig. 25.

To maximize the benefits for this configuration, several desirable geometrical attributes will lead to an optimized design in terms of film-cooling coverage. These are 1) reduction of pressure-side lip thickness t and 2) enlargement of slot s, provided that both are consistent with structural strength requirements. The combination of geometrical attributes 1 and 2 can then lead to minimum cooling flow rates for the pressure-side cutback trailing-edge configurations. The limit on the cooling flow rate would then come from the metal temperature ahead of the cutback distance. Because the metal temperature increases monotonically with distance from the supply cavity up to the cutback distance from the trailing edge, the effect of trailing-edge film cooling takes place after this point.

The metal temperature profile with pressure-side cutback might not increase monotonically toward the trailing edge as it is the case for the centerline discharge configurations. The surface of the pressure-side land could also be made aerodynamically rough to enhance the coolant heat-transfer coefficient on that surface. Thus, the preferred selection of distance x, lip thickness t, slot s, and blowing parameter M leads to a pressure-side cutback trailing-edge configuration, which becomes attractive for airfoil durability and overall aerodynamic performance. This paper has summarized insight into the relevant characteristics affecting the design of trailing-edge configurations for high-pressure turbine airfoils.

Conclusions

Two set of conclusions are derived from this treatment: 1) conclusions from the analytical development and 2) conclusions from the experimental techniques presented.

In the analytical development, closed-form, analytical models of airfoil temperature for four most representative trailing-edge configurations were presented. These include 1) solid wedge shape without discharge, 2) wedge with centerline slot discharge, 3) wedge with centerline discrete-hole discharge, and 4) wedge with pressure-side cutback slot discharge. These analytical solutions for metal temperature provide fundamental insight into the relevant characteristics affecting the design of trailing-edge configurations for high-pressure turbine airfoils.

Based on the information gained from the analysis the relevant design features can be summarized as follows: 1) size of the cooling passage; 2) internal cooling features inside the cooling passage; 3) trailing-edge thickness; 4) pressure-side lip thickness; 5) roughness on pressure-side land; and 6) slot film coverage. From this set of features, only two, namely, 1 and 2, can be used effectively for centerline discharge configurations, whereas all features, 1–6, can be used effectively for the pressure-side cutback configurations. For the cutback design, there are also the added benefits of improved aerodynamic performance caused by thinner trailing edges. The life capability to resist thermal-mechanical fatigue and creep is also improved as metal temperature distributions are more evenly distributed over the entire trailing-edge region for the cutback designs.

Overall design parameters were introduced to illustrate how these parameters can be selected during the optimization cycle for the trailing-edge designs. This process leads to the search of detail design features and geometrical attributes, which can be judiciously selected in concert with the available design space. In this regard, cooling effectiveness becomes a strong function of the convective efficiency using internal cooling features to temper stepwise pressure and coolant Mach-number distributions inside the trailing-edge passages. The film-cooling effectiveness and corresponding film coverage defined in terms of geometrical lip-to-slot ratio t/s and blowing ratio are also important design parameters. These are influential in maintaining desired film-cooling effectiveness while minimizing trailing-edge cooling flow for specified trailing-edge cutback distances.

In the experimental development, the heat transfer in both the internal cooling chamber and cutback land of an airfoil trailing edge with internal pedestals or pin fins is presented. For internal cooling, the last row, row 5, where the oblong shaped teardrop begins, has a relatively low level of heat-transfer enhancement compared with the previous fourth row of pedestals, but still comparable with row 3. Compared with smooth channel, the magnitude of the enhancement for the entire heat-transfer domain ranges from 2.4 to 3.3 for $3.5 \times 10^3 < Re < 9.5 \times 10^3$. The enhancement is at least 10% higher than uniform pin fin for $Re < 9.5 \times 10^3$. As for the heat transfer over the cutback land, when blowing ratio $M > 1.32$, the protection is much effective for $x/s < 7.5$. The effect of the nonuniform coolant distribution on the cooling performance is observed when the blowing ratio is relatively small.

References

[1]Kuhne, C. M., "Reduced Shock Transonic Airfoil," U.S. Patent 2003/0072649A1, April 2003.

[2]Eisemann, K. M., "Uncooled Data Reduction," Pratt & Whitney Internal Documentation, Pratt & Whitney, East Hartford, CT, June 2003.

[3]Karamcheti, K., *Principles of Ideal-Fluid Aerodynamics*, Krieger, Malabar, FL, 1980, Chap. 13.

[4]Holloway, D. S., Leylek, J. H., and Buck, F. A., "Pressure Side Bleed Film Cooling: Part 1—Unsteady Framework for Experimental and Computational Results," American Society of Mechanical Engineers, GT-2002-30472, June 2002.

[5]Maclachlan, D. W., and Knowles, D. M., "The Effect of Material on the Analysis of Single Crystal Turbine Blades: Part I—Material Model," *Fatigue and Fracture Engineering Material Science*, Vol. 25, Nov. 2002, pp. 385–398.

[6]Maclachlan, D. W., and Knowles, D. M., "The Effect of Material on the Analysis of Single Crystal Turbine Blades: Part II—Component Analysis," *Fatigue and Fracture Engineering Material Science*, Vol. 25, Nov. 2002, pp. 385–398.

[7]Taslim, M. E., Spring, S. D., and Mehlman, B. P., "Experimental Investigation of Film Cooling Effectiveness for Slots of Various Exits Geometries," *Journal of Thermophysics and Heat Transfer*, Vol. 6, No. 2, 1992, pp. 302–307.

[8]Sivasegaram, S., and Whitelaw, J. H., "Film Cooling Slots: The Importance of Lip Thickness and Injection Angle," *Journal of Mechanical Engineering Science*, Vol. 11, No. 1, 1969, pp. 22–27.

[9]Burns, W. K., and Strollery, J. L., "The Influence of Foreign Gas Injection and Slot Geometry on Film Cooling Effectiveness," *International Journal of Heat Mass Transfer*, Vol. 12, Aug. 1969, pp. 935–951.

[10]Pai, B. R., and Whitelaw, J. H., "The Prediction of Wall Temperature in the Presence of Film Cooling," *International Journal of Heat Mass Transfer*, Vol. 14, March 1971, pp. 409–426.

[11]Kacker, S. C., and Whitelaw, J. H., "An Experimental Investigation of Slot Lip Thickness on the Impervious Wall Effectiveness of the Uniform Density, Two-Dimensional Wall Jet," *International Journal of Mass Heat Transfer*, Vol. 12, Sept. 1969, pp. 1196–1201.

[12]Uzol, O., and Camci, C., "Aerodynamic Loss Characteristics of a Turbine Blade with Trailing Edge Coolant Ejection: Part 2—External Aerodynamics, Total Pressure Losses, and Predictions," *Journal of Turbomachinery*, Vol. 123, April 2001, pp. 249–257.

[13]Uzol, O., Camci, C., and Glezer, B., "Aerodynamic Loss Characteristics of a Turbine Blade with Trailing Edge Coolant Ejection: Part 1—Effect of Cutback Length, Spanwise Rib Spacing, Free-Stream Renolds Number, and Chordwise Rib Length on Discharge Coefficients," *Journal of Turbomachinery*, Vol. 123, April 2001, pp. 238–248.

[14]Holloway, D. S., Leylek, J. H., and Buck, F. A., "Pressure Side Bleed Film Cooling: Part 1—Steady Framework for Experimental and Computational Results," American Society of Mechanical Engineers, GT-2002-30471, June 2002.

[15]Chyu, M. K., Uysal, U., and Li, P.-W., "Convective Heat Transfer in a Triple-Cavity Structure near Turbine Blade Trailing Edge," *Proceedings of IMECE'02, International Mechanical Engineers Congress*, IMECE 2002-32405, ASME, New York, 2002.

[16]Martini, P., and Schulz, A., "Experimental and Numerical Investigation of Trailing Edge Film Cooling by Circular Coolant Wall Jets Ejected from a Slot with Internal Rib Arrays," *Journal of Turbomachinery*, Vol. 126, No. 2, 2004, pp. 229–236.

[17]Kim, Y. W., Chad, C., and Moon, H. K., "Film Cooling Characteristics of Pressure Side Discharge Slots in an Accelerating Mainstream Flow," *Proceedings of GT2005, ASME Turbo Expo 2005: Power for Land, Sea and Air*, GT 2005-69061, ASME, New York, June 2005.

[18]Martini, P., Schulz, A., and Bauer, H. J., "Film Cooling Effectiveness and Heat Transfer on the Trailing Edge Cutback of Gas Turbine Airfoils with Various Internal Cooling Designs," *Proceedings of GT2005, ASME Turbo Expo 2005: Power for Land, Sea and Air*, GT 2005-68083, ASME, New York, June 2005.

[19]Cunha, F. J., Dahmer, M. T., and Chyu, M. K., "Analysis of Airfoil Trailing Edge Heat Transfer and Its Significance in Thermal-Mechanical Design and Durability," *Proceedings of GT2005, ASME Turbo Expo 2005: Power for Land, Sea and Air*, GT 2005-68016, ASME, New York, June 2005.

[20]Vedula, R. J., and Metzger, D. E., "A Method for Simultaneously Determination of Local Effectiveness and Heat Transfer Distribution in Three-Temperature Convection Situations," American Society of Mechanical Engineers, Paper 91-GT-345, June 1991.

[21]Ekkad, S. V., Zapata, D., and Han, J. C., "Heat Transfer Coefficients over a Flat Surface with Air and CO_2 Injection Through a Compound Angle Holes Using a Transient Liquid Crystal Image Method," *Journal of Turbomachinary*, Vol. 119, No. 4, 1997, pp. 580–586.

[22]Ekkad, S. V., Zapata, D., and Han, J. C., "Film Effectiveness over a Flat Surface with Air and CO_2 Injection Through a Compound Angle Holes Using a Transient Liquid Crystal Image Method," *Journal of Turbomachinary*, Vol. 119, 1997, pp. 587–593.

[23]Yu, Y., Yen, C.-H., Shih, T. I.-P., Chyu, M. K., and Gogineni, S., "Film Cooling Effectiveness and Heat Transfer Coefficient Distributions Around Diffusion Shaped Holes," *Journal of Heat Transfer*, Vol. 124, Oct. 2002, pp. 820–827.

[24]Chyu, M. K., and Ding, H., "Heat Transfer in a Cooling Channel with Vortex Generators," *Journal of Heat Transfer*, Vol. 119, No. 2, 1997, p. 206.

[25]Chyu, M. K., "Heat Transfer and Pressure Drop for Short Pin-Fin Arrays with Pin-Endwall Fillet," *Journal of Heat Transfer*, Vol. 112, Nov. 1990, pp. 926–932.

[26]Kline, S. J., and McClintock, F. A., "Describing Uncertainties in Single Sample Experiments," *Mechanical Engineering (American Society of Mechanical Engineers)*, Vol. 75, 1953, pp. 3–8.

[27]Goldstein, R. J.,"Film Cooling," *Advance Heat Transfer*, Vol. 7, Jan. 1971, pp. 321–379.

[28]Metzger, D. E., Carper, H. J., and Swank, L. R.,"Heat Transfer with Film Cooling near Nontangential Injection Slots," *Journal of Engineering Power*, Vol. 90, 1968, pp. 157–163.

[29]Sen, B., Schmidt, D. L., and Bogard, D. G., "Film Cooling with Compound Angle Holes: Heat Transfer," *Journal of Turbomachinery*, Vol. 118, No. 4, 1996, pp. 800–806.

[30]Langston, L., "A Year of Turbulence," *Power and Energy, ASME Magazine*, June 2004, pp. 29–33.

[31]Cunha, F. J., "Integrated Steam/Gas Cooling System for Gas Turbines," U.S. Patent 5,340,274, Aug. 1994.

[32]Lee, C.-P., "Turbine Blade Trailing Edge Cooling Openings and Slots," U.S. Patent 6,174,135B1, 16 Jan. 2001.

[33]Jacala, A., Davis, R. M., Sullivan, M. A., Chyu, R. P., and Staub, F., "Closed Circuit Steam Cooled Bucket," U.S. Patent 5,536,143, July 1996.

[34]Cunha, F. J., DeAngelis, D. A., Brown, T. A., Chopra, S., Correia, V. H. S., and Predmore, D. R., "Turbine Stator Vane Segments Having Combined Air and Steam Cooling Circuits," U.S. Patent 5,634,766, 1997.

[35]Cunha, F. J., Dahmer, M. T., and Chyu, M. K., "Thermal-Mechanical Life Prediction System for Anisotropic Turbine Components," IGTI/ASME Paper GT2005-68107, June 2005.

[36]Braddy, B. T., "Film Cooled Airfoil Body," U.S. Patent 4,303,374, Dec. 1981.

[37]Starkweather, J. H., "Turbine Blade," U.S. Patent 5,813,836, Sept. 1998.

[38]Manning, R. F., Acquaviva, P. J., and Demers, E., "Series Impingement Cooled Airfoil," U.S. Patent 6036441, 1981.

[39]Cunha, F. J., and DeAngelis, D. A., "Cooling Circuits for Trailing Edge Cavities in Airfoils," U.S. Patent 6,056,505, May 2000.

[40]Hill, E. C., Liang, G. P., and Auxier, T., "Airfoil Trailing Edge Cooling Arrangement," U.S. Patent 4,601,638, July 1986.

[41]Zukauskas, A. A., "Heat Transfer from Tubes in Cross Flow," *Advances in Heat Transfer*, Vol. 8, Jan. 1972, pp. 116–133.

[42]Ishida, K., and Hamabe, K., "Effect of Pin-Fin Aspect Ratio and Arrangement on Heat Transfer and Pressure Drop of Pin Fin Duct for Airfoil Internal Cooling Passage," American Society of Mechanical Engineers, Paper 85-WA/HT-62, May 1985.

[43]Han, J. C., Dutta, S., and Ekkad, S., *Gas Turbine Heat Transfer and Cooling Technology*, 1st ed., Taylor and Francis, New York, 2000, Chap. 1.

[44]Eckert, E. R. G., "Analogies to Heat Transfer Processes," *Measurements in Heat Transfer*, edited by E. R. G. Eckert and R. J. Goldstein, Hemisphere, New York, 1976, Chap. 1.